AGU PUBLICATIONS

Paleoceanography

RESEARCH ARTICLE
10.1002/2016PA003032

Key Points:
- The TEX_{86} signal exported to the sediments in the Gulf of Mexico is an integrated shallow subsurface mean annual temperature signal
- Alkenone-based $U^{K'}_{37}$ covaries with SST over the 4 year sampling interval, but the $U^{K'}_{37}$ in the Gulf of Mexico represents mean annual SST, and the $U^{K'}_{37}$ covaries with SST over the 4 year sampling interval, but the $U^{K'}_{37}$-SST relationship in the GoM is nonlinear above 24°C
- Despite being sourced from the subsurface, the TEX_{86} can still be used to reconstruct SSTs on interannual to centennial timescales

Supporting Information:
- Supporting Information S1

Correspondence to:
J. N. Richey,
jrichey@usgs.gov

Citation:
Richey, J. N., and J. E. Tierney (2016), GDGT and alkenone flux in the northern Gulf of Mexico: Implications for the TEX_{86} and $U^{K'}_{37}$ paleothermometers, *Paleoceanography*, *31*, 1547–1561, doi:10.1002/2016PA003032.

Received 2 SEP 2016
Accepted 21 NOV 2016
Accepted article online 24 NOV 2016
Published online 19 DEC 2016

GDGT and alkenone flux in the northern Gulf of Mexico: Implications for the TEX_{86} and $U^{K'}_{37}$ paleothermometers

Julie N. Richey[1] and **Jessica E. Tierney**[2,3]

[1]U.S. Geological Survey, St. Petersburg, Florida, USA, [2]Department of Geosciences, University of Arizona, Tucson, Arizona, USA, [3]Woods Hole Oceanographic Institution, Woods Hole, Massachusetts, USA

Abstract The TEX_{86} and $U^{K'}_{37}$ molecular biomarker proxies have been broadly applied in downcore marine sediments to reconstruct past sea surface temperature (SST). Although both TEX_{86} and $U^{K'}_{37}$ have been interpreted as proxies for mean annual SST throughout the global ocean, regional studies of glycerol dibiphytanyl glycerol tetraethers (GDGTs) and alkenones in sinking particles are required to understand the influence of seasonality, depth distribution, and diagenesis on downcore variability. We measure GDGT and alkenone flux, as well as the TEX_{86} and $U^{K'}_{37}$ indices in a 4 year sediment trap time series (2010–2014) in the northern Gulf of Mexico (nGoM), and compare these data with core-top sediments at the same location. GDGT and alkenone fluxes do not show a consistent seasonal cycle; however, the largest flux peaks for both occurs in winter. $U^{K'}_{37}$ covaries with SST over the 4 year sampling interval, but the $U^{K'}_{37}$-SST relationship in this data set implies a smaller slope or nonlinearity at high temperatures when compared with existing calibrations. Furthermore, the flux-weighted $U^{K'}_{37}$ value from sinking particles is significantly lower than that of underlying core-top sediments, suggesting preferential diagenetic loss of the tri-unsaturated alkenone in sediments. TEX_{86} does not covary with SST, suggesting production in the subsurface upper water column. The flux-weighted mean TEX_{86} matches that of core-top sediments, confirming that TEX_{86} in the nGoM reflects local planktonic production rather than allochthonous or in situ sedimentary production. We explore potential sources of uncertainty in both proxies in the nGoM but demonstrate that they show nearly identical trends in twentieth century SST, despite these factors.

1. Introduction

Lipid biomarker sea surface temperature (SST) proxies such as the TEX_{86} and $U^{K'}_{37}$ have some advantages over foraminiferal geochemistry in that they can be applied in regions of the ocean where carbonate is not well preserved or where planktic foraminifera are not abundant. More importantly, they augment the suite of SST proxies that are available for multiproxy paleoceanographic reconstruction. Each of the geochemical SST proxies is subject to varying degrees of nontemperature overprints (e.g., salinity, pH, and redox conditions), diagenetic alteration, and ecological biases that may limit its efficacy in accurately reflecting past temperature variability. The relative influences of these factors can vary regionally, rendering local water column and core-top studies valuable for interpreting SST proxy records and understanding discrepancies between different types of contemporaneous proxy records.

Long-chain alkenones are membrane lipids produced by haptophyte algae and are ubiquitous in global marine sediments. The $U^{K'}_{37}$ index is based on the observation that haptophytes produce more di-unsaturated C_{37} alkenone ($C_{37:2}$) relative to tri-unsaturated ($C_{37:3}$) with increasing growth temperature [*Brassell et al.,* 1986]. A linear relationship between the $U^{K'}_{37}$ index and water temperature was experimentally determined in culture studies of *Emiliania huxleyi* [*Prahl et al.,* 1988] and in global core-top calibrations [*Müller et al.,* 1998; *Conte et al.,* 2006]. Despite the widespread validation of this relationship, some studies have found discrepancies between coeval alkenone and other SST proxy data [*Huguet et al.,* 2006; *Liu et al.,* 2009; *Castañeda et al.,* 2010; *Rommerskirchen et al.,* 2011; *Seki et al.,* 2012]. These offsets may arise from location-specific seasonal biases in alkenone production [*Rosell-Melé and Prahl*, 2013], diagenetic alteration of the alkenone signal [*Conte et al.,* 2006], or lateral transport of alkenones from distal locations in the fine sediment fraction [*Mollenhauer et al.,* 2008]. A number of experiments have also documented nonthermal influences on the $U^{K'}_{37}$ of alkenones grown under isothermal conditions such as light and nutrient limitation [*Epstein et al.,* 1998, 2001; *Prahl et al.,* 2003; *Yamamoto et al.,* 2000].

The TEX_{86} index is based on the cyclopentane ring distribution of isoprenoid glycerol dibiphytanyl glycerol tetraethers (isoGDGTs). In most marine environments, isoGDGTs are primarily produced by a group of marine ammonia oxidizing archaea called Thaumarchaeota [*Damsté et al.,* 2002], although there may also be contributions from planktonic Euryarchaeota [*Lincoln et al.,* 2014] and benthic methanotrophic archaea [*Zhang et al.,* 2011]. The TEX_{86} index is strongly correlated with upper ocean water temperatures in global core-top calibration studies [*Kim et al.,* 2010; *Tierney and Tingley,* 2014, 2015], and in the water column [*Wuchter et al.,* 2006; *Schouten et al.,* 2012] despite the fact that GDGTs are produced by a broad range of marine archaea living throughout the water column [*Zhu et al.,* 2016], and in subsurface sediments [*Lipp et al.,* 2008]. Recent culture studies, while confirming that increased temperatures lead to an increase in the TEX_{86} index, have found evidence that low oxygen [*Qin et al.,* 2015] and/or low nitrification rates [*Hurley et al.,* 2016] are also associated with increased cyclization and therefore may influence the TEX_{86} index. A better understanding of the mechanisms controlling the distribution of GDGTs is needed to interpret discrepancies between coeval TEX_{86} and Mg/Ca [*Richey et al.,* 2011] or TEX_{86} and $\mathbf{U}^{\mathbf{K}'}_{37}$-based SST reconstructions [*Huguet et al.,* 2006; *Liu et al.,* 2009; *Castañeda et al.,* 2010; *Rommerskirchen et al.,* 2011; *Seki et al.,* 2012; *Tierney et al.,* 2016].

We evaluate controls on the TEX_{86} and $\mathbf{U}^{\mathbf{K}'}_{37}$ paleothermometers in the northern Gulf of Mexico (nGoM) by quantifying the seasonal flux of alkenones and GDGTs in a weekly-to-monthly resolution 4 year (2010–2014) sediment trap time series. We then compare the TEX_{86} and $\mathbf{U}^{\mathbf{K}'}_{37}$ of sinking particles to that of underlying sediments from a series of multicores collected from the sediment trap site.

2. Hydrographic Setting

The Gulf of Mexico is part of the Atlantic Warm Pool, an annual feature defined by the $\geq$28.5°C isotherm encompassing the western tropical Atlantic, Caribbean Sea, and Gulf of Mexico [*Wang et al.,* 2008]. The loop current brings warm salty Caribbean surface water into the nGoM through the Yucatan Channel and out through the Florida Straits, where it forms the Gulf Stream, transporting heat and salt poleward in the North Atlantic. The loop current penetrates farther north and west into the nGoM during the summer and can propagate warm salty water to the northwestern most nGoM via the sporadic separation of "warm core" anticyclonic eddies every 6–17 months [*Vukovich*, 1995]. Cold core or cyclonic eddies form on the eastern and northern periphery of the loop current and can be responsible for transporting relatively cool and fresh coastal waters offshore [*Walker et al.,* 2011].

The sediment trap is located in the oligotrophic outer continental slope, 120 nautical miles southwest of the Mississippi River Delta. The climatological surface salinity varies between 35.5 and 36.5, with highest salinity in winter and lowest in summer [*Balmaseda et al.,* 2012]. Anomalous low salinity lenses were observed in the upper 0–10 m of the water column during conductivity-temperature-depth (CTD) casts at the site in July 2008 (31.2 practical salinity unit (psu)) and September 2010 (34.4 psu). July of 2008 followed extreme spring flooding in the Mississippi drainage basin with river discharge rates more than double the climatological rates [*Kourafalou and Androulidakis*, 2013], and an exceptionally large Mississippi plume was observed through July [*Shi and Wang*, 2009]. Satellite altimetry indicates the presence of a "cold core" or cyclonic eddy over the sediment trap site in September 2010. These mesoscale circulation features can entrain cooler, fresher, and more nutrient-rich shelf waters and move them offshore [*Walker et al.,* 2011; *Huang et al.,* 2013], influencing local productivity.

The annual cycle in climatic mean monthly SST varies between 19°C and 31°C (from Hadley Centre sea ice and sea surface temperature (HadISST)) [*Rayner et al.,* 2003]. The mixed layer depth (MLD) at the study site, as measured by CTD casts during sediment trap deployments/recoveries, varies between 25 m in the summer and 120 m in winter [*Reynolds and Richey*, 2016]. Primary productivity in the offshore nGoM is highest in winter, when wind-driven mixing of the upper water column is greatest. *Muller-Karger et al.* [2015] found a significant positive correlation between MLD and chlorophyll α concentration in the nGoM over the past two decades. Organic carbon and mass flux rates in the sediment trap reflect this seasonal cycle in primary productivity, with maximum flux rates usually occurring in winter (December–February (DJF)), and minima in summer (June–August (JJA)) [*Richey et al.,* 2014]. There is an exceptionally high flux in late August of 2012, directly following Hurricane Isaac, which passed over the sediment trap site on 27 August 2012.

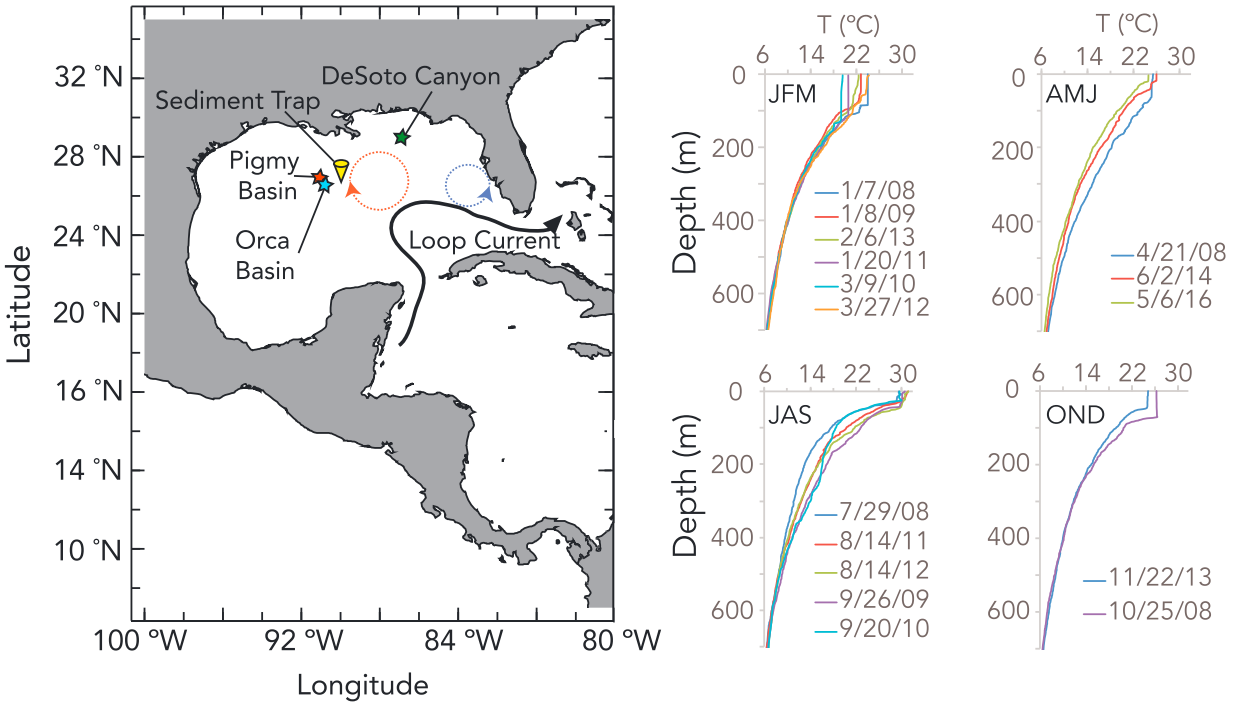

Figure 1. Location of the sediment trap and Gulf of Mexico coring locations referenced in the discussion (Pigmy Basin-red, Orca Basin-blue, and DeSoto Canyon-green). A cartoon of the loop current position, as well as a warm-core eddy (red), and a cold-core eddy (blue) are drawn. Vertical temperature profiles of the upper 700 m of the water column for CTD casts at the sediment trap site 2008–2013. Winter (DJF), spring (March–May), summer (JJA), and fall (September–November) profiles are shown in separate panels.

Another factor that may contribute to anomalies in local primary productivity is the close proximity of the sediment trap to the Green Canyon reservoir, where episodic oil seeps can cause local upwelling of nutrient rich deep water [*D'souza et al.,* 2016]. Note that the Deepwater Horizon oil spill occurred during our sampling period in April of 2010, 222 km northeast of the sediment trap site.

3. Methods

3.1. Sediment Trap

The McLane PARFLUX Mark 78 automated sediment trap is moored at 700 m water depth in the northern Gulf of Mexico (27.5°N and 90.3°W) in 1150 m water depth (Figure 1). The trap is equipped with 21 collection cups, all mounted on a rotating plate programmed to rotate every 7 to 14 days. Sample cups were prefilled with a buffered formalin solution made with filtered seawater, formalin (3.7%), and sodium borate. The trap was recovered and redeployed every 6–9 months, and a sampling gap occurred between early February 2012 and late March 2012. Sediment-trap samples were wet split into four aliquots using a precision rotary splitter at the University of South Carolina, stored in buffered, deionized water, and then refrigerated. Methods and data for bulk sediment analysis of sediment trap samples (i.e., mass flux and total organic carbon flux) are described in *Richey et al.* [2014].

3.2. Sediment Cores

Multicores were collected in 2013 at the sediment trap site, in 1150 m water depth. Cores each had an intact sediment-water interface and were extruded and subsampled onboard at 5 mm intervals directly following collection. A ^{210}Pb chronology was developed for one of the subcores (GMT14-MC3J) and indicates a sedimentation rate of 58 cm/kyr (see the supplementary information for details). The resulting age-depth model was applied to the three additional subcores analyzed in tandem for downcore biomarker work (GMT14-MC3K, GMT14-MC4R, and GMT14-MC4S). Sediment samples were freeze-dried, homogenized, then underwent the same extraction and column chromatography procedure as sediment trap filters.

3.3. Biomarker Analysis

Sediment trap samples were filtered onto 0.7 μm precombusted glass fiber filters (GF/F), freeze-dried, then extracted using a Dionex Accelerated Solvent Extractor (ASE 200) in 9:1 methylene chloride (DCM) to methanol (MeOH). The total lipid extract was separated into acid and neutral fractions using aminopropyl gel columns, with neutrals eluting in 3:1 DCM:isopropanol and acids eluting in 4% acetic acid in DCM. The neutral fraction was then separated into hydrocarbon, ketone, and polar fractions via silica gel column chromatography using the elution scheme: hexane (hydrocarbons), DCM (alkenones), and MeOH (GDGTs). Note that this procedure only isolates core GDGT lipids; intact polar GDGTs were not analyzed in this study.

The polar fraction, containing the GDGTs, was dissolved in a 99:1 (vol:vol) mixture of hexane:isopropanol, then filtered through 0.45 μm polytetrafluoroethylene filters. Analyses of GDGTs for TEX_{86} and branched-to-isoprenoid tetraether (BIT) index determination were performed by high-performance liquid chromatography-mass spectrometry (HPLC-MS) at Woods Hole Oceanographic Institution. Samples were analyzed on an Agilent 1260 HPLC coupled to an Agilent 6120 MSD according to the method of *Schouten et al.* [2007]. Briefly, A Prevail Cyano column (150 × 2.1 mm, 3 μm) was used with 100% hexane (A) and 90:10 hexane:isopropanol (v:v) (B) as eluents. Samples were injected then eluted isocratically for the first 5 min with A, after which the eluent increased by a linear gradient up to 18% B over the next 35 min at a flow rate of 0.2 mL/min. Detection was performed in single ion monitoring mode. Synthetic C_{46} GDGT obtained from Purdue University was used as an internal quantification standard. All GDGT samples were analyzed in duplicate. Long-term analyses of an external laboratory standard yield a precision of 0.004 TEX_{86} units.

Alkenone fractions were analyzed via gas chromatography with a flame ionization detector (GC-FID) at the U.S. Geological Survey St. Petersburg Coastal and Marine Science Center. GC-FID conditions were split/splitless injection (inlet temperature: 300°C), DB-1 capillary column (60 m, 0.32 mm i.d., 0.10 μm film thickness), 1.5 mL/min He carrier gas, with 1 μl sample injection volume, and the following oven temperature program: 60°C to 270°C at 30°C/min, 270°C to 310°C at 1.2°C/min, and 310°C to 325°C at 10°C/min. Identification of alkenones was verified using GC-MS (Agilent 7890B gas chromatograph coupled to an Agilent 5977A mass spectrometer with the same column and method) and based on comparison with a purified alkenone standard from cultured *Emiliania huxleyi*. Both hexatriacontane and heptatriacontane were added to samples as internal quantification standards for alkenones. All new data presented in this study can be accessed in the USGS Data Release [*Richey and Tierney*, 2016].

3.4. Statistical Assessment

Relationships between sediment trap variables were assessed by calculating Pearson product-moment correlation coefficients. Significance of these correlations was determined using a nonparametric method that accounts for reduced degrees of freedom due to serial correlation [*Ebisuzaki*, 1997].

4. Results and Discussion

4.1. Alkenone Flux

Annual alkenone flux is slightly weighted toward winter production, but there is no consistent seasonal cycle (Figure 2d). Overall, alkenone flux is closely tied to total mass flux and total organic carbon (TOC) flux in the 2010–2014 sediment trap time series (Figure 3a). The mean flux of C_{37} alkenone is 1.4 $\mu g\, m^{-2}\, d^{-1}$, with peak fluxes of 4–9 $\mu g\, m^{-2}\, d^{-1}$ (Figure 2). Individual flux peaks can account for up to 25% of the annual flux during a 2 week period (e.g., January 2010 and September 2012). Although alkenones are continuously exported to the sediments throughout the year, the highest flux occurs in winter, with January accounting for more than 20% of the annual flux each year. This is consistent with maximum organic carbon flux in the winter [*Richey et al.,* 2014] and an observed winter peak in primary productivity in the offshore oligotrophic Gulf of Mexico [*Muller-Karger et al.,* 2015]. This is in contrast to the assumption that alkenone production is spring-summer weighted at other sites in the global ocean [*Brassell et al.,* 1986; *Conte et al.,* 1992; *Brassell*, 1993; *Sikes et al.,* 2002; *Martínez-Garcia et al.,* 2009; *Leduc et al.,* 2010; *Schneider et al.,* 2010] and underscores the importance of regional sediment trap studies in interpreting proxy seasonality.

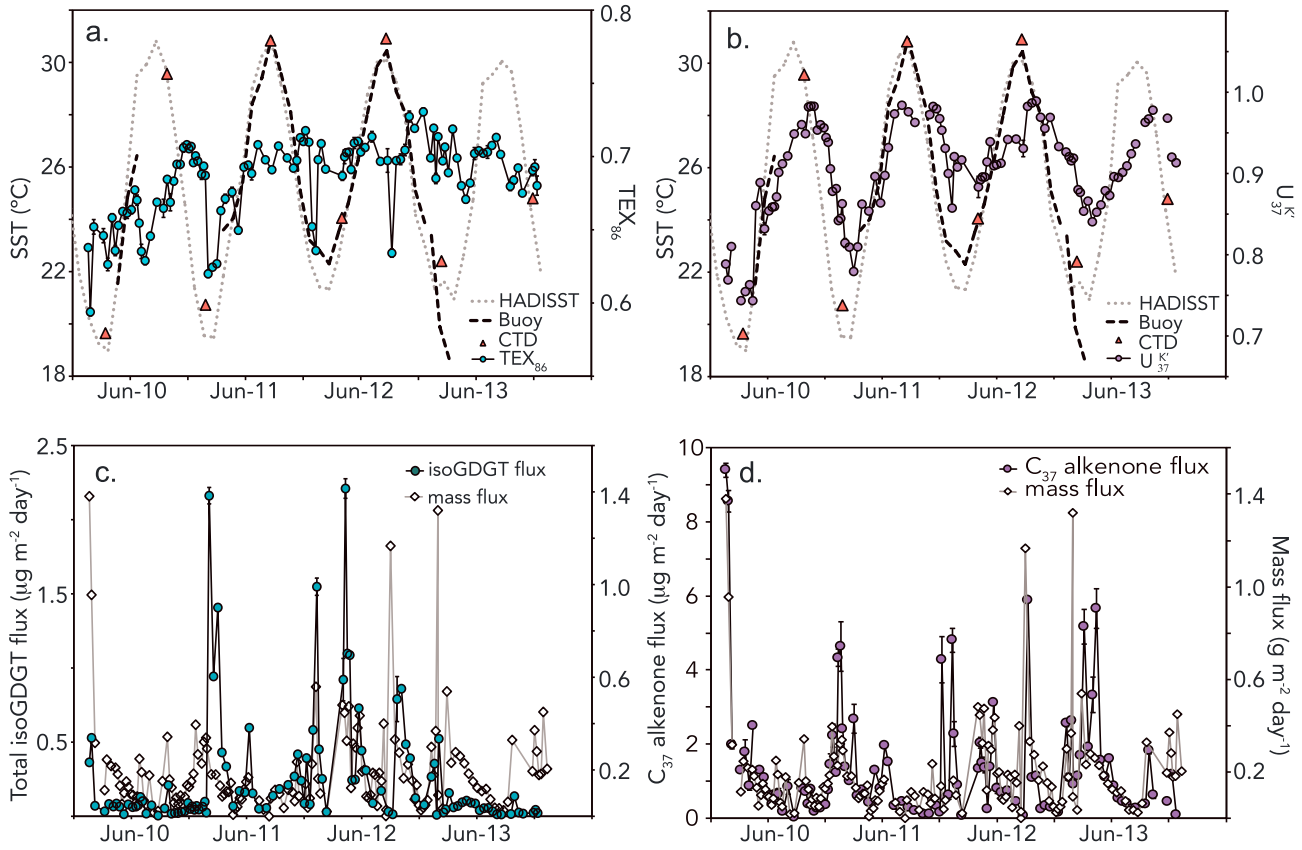

Figure 2. Time series of (a) TEX_{86} and (b) $U^{K'}_{37}$ in sinking particles, and flux of (c) GDGTs and (d) alkenones at 700 m water depth in the northern Gulf of Mexico. SST from HadISST (grey dashed line), local buoy data (black dashed line), and CTD casts during sediment trap recovery/deployment cruises is shown in Figures 2a and 2b. Total flux of isoprenoid GDGTs ($\Sigma_{GDGT\ 0,\ I,\ II,\ III,\ V\ and\ V'}$) (Figure 2c) and C_{37} alkenone ($\Sigma C_{37:3}$, $C_{37:2}$) (Figure 2d) are plotted with the total mass flux [*Richey et al.*, 2014] from January 2010 to December 2013.

4.2. GDGT Flux

The mean flux of isoprenoid GDGTs (isoGDGTs) is 0.26 $\mu g\, m^{-2}\, d^{-1}$, with peak fluxes of 0.5–2.2 $\mu g\, m^{-2}\, d^{-1}$ (Figure 2). Although some isoGDGT flux peaks co-occur with peaks in mass flux, isoGDGT flux does not vary in proportion to mass flux or TOC flux (Figures 3d and 3e). Similar to alkenones, GDGT flux is winter weighted, with DJF flux accounting for 40–60% of the annual flux. During three of the four sampling years, 25% of the annual flux of isoGDGTs occurred in January (2012 had a large spring isoGDGT flux event). The mean concentration of isoGDGTs in sinking particles is 4 $\mu g\, g^{-1}$ sediment and varies between 0.4 and 21 $\mu g\, g^{-1}$ sediment. The percentage of terrigenous material in sinking particles varies between 2% and 40% [*Richey et al.*, 2014]. The flux of branched GDGTs (brGDGTs) measured in the sediment trap samples is low, varying between 0 and 18.7 $ng\, m^{-2}\, d^{-1}$, with an average flux of 1.6 $ng\, m^{-2}\, d^{-1}$ over the 4 year sampling interval. Unlike isoGDGT flux, brGDGT flux varies weakly in proportion to mass flux (Figure 3f). The branched-to-isoprenoid tetraether (BIT) index, a metric for inferring the relative contribution of terrestrially derived branched GDGTs [*Hopmans et al.*, 2004], varies minimally between 0 and 0.02 in sediment trap samples, with the exception of a single peak of 0.07 in August of 2012 (not shown).

4.3. $U^{K'}_{37}$ SST Estimates

The $U^{K'}_{37}$ values of sinking particles display a seasonal cycle that closely follows SST, varying between 0.75 and 0.99 during the 2010–2014 sampling interval (Figure 2b). Summer maxima are consistently near saturation at 0.98–0.99, while the winter minima display considerable interannual variability between 0.74 and 0.85. This is reflective of instrumental observations in the northern Gulf of Mexico. Both the HadISST and nearby buoy data record consistent summer maxima of 30.4°C (±0.4°C), with large interannual variability in winter minima

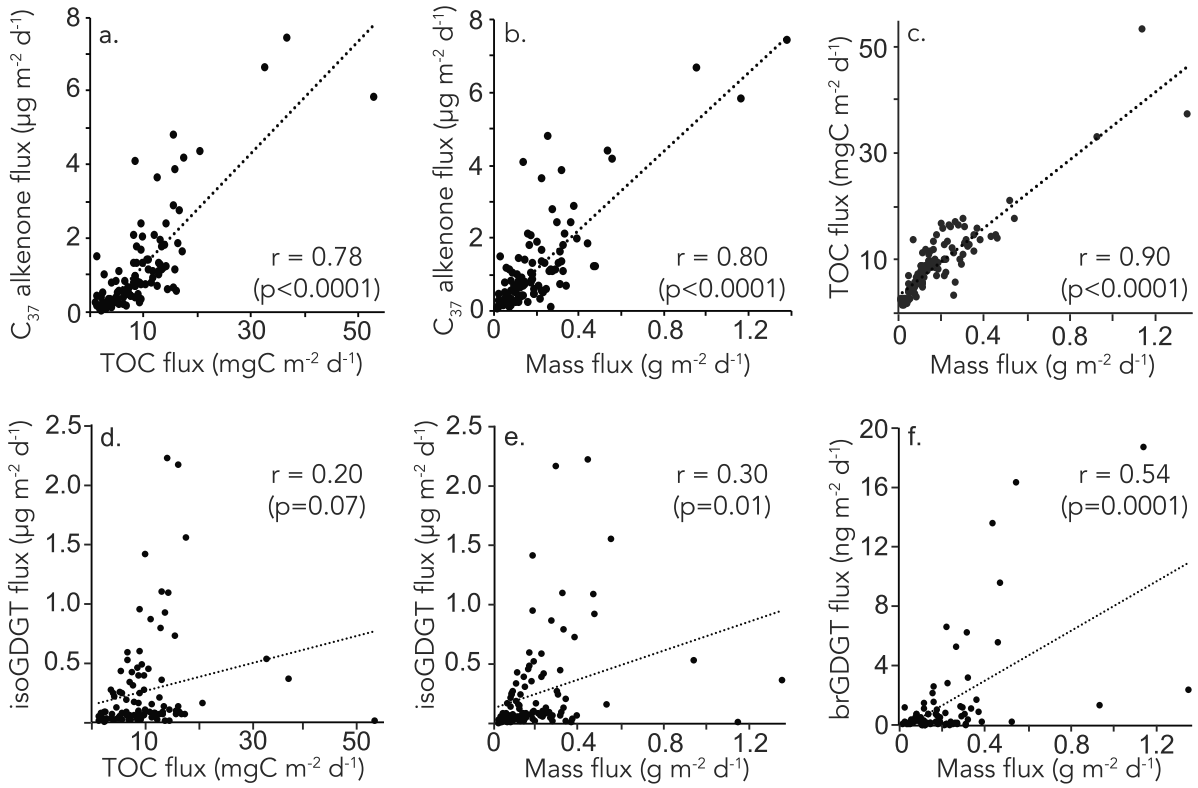

Figure 3. In the Gulf of Mexico sediment trap. (a) The flux of $C_{37:2}$ alkenones versus total organic carbon (TOC) flux, (b) flux of $C_{37:2}$ alkenones versus mass flux, and (c) TOC flux versus mass flux. (d) Total isoprenoid GDGT flux versus TOC, (e) total isoprenoid GDGT flux versus mass flux, and (f) total branched GDGT flux versus mass flux.

(Figure 2). For example, the monthly minimum for the winter of 2009–2010 is 19.2°C and the monthly minimum for 2011–2012 is 21.7°C. This unusually cold winter of 2009–2010 is reflected in the lowest $\mathbf{U}^{\mathbf{K}'}_{37}$ values in the 4 year time series and is a documented cold event throughout the North Atlantic Basin [*Bryden et al.,* 2014].

The $\mathbf{U}^{\mathbf{K}'}_{37}$ time series has a maximum correlation ($r = 0.82$, $p < 0.0001$) with overlying SST at a lag of 28 days, implying a ~34 m d^{-1} sinking rate (0–700 m), which is within the range observed for other sites in the Atlantic [*Müller and Fischer*, 2001; *Fischer and Karakas*, 2009; *Mollenhauer et al.,* 2015]. The covariance of the $\mathbf{U}^{\mathbf{K}'}_{37}$ in sinking particles with overlying SST indicates a rapid response of coccolithophorids to the seasonal succession in SST, and continuous export of that signal to the sediments, regardless of productivity or overall flux. The flux-weighted mean $\mathbf{U}^{\mathbf{K}'}_{37}$ value over the 4 year sampling interval is 0.88, equivalent to an SST of 24.8°C using the *Prahl et al.* [1988] equation and 24.6°C using the *Sonzogni et al.* [1997] equation. This is slightly cooler than the mean annual instrumental SST over that same interval (25.4°C) and reflects the higher winter/spring flux in the northern Gulf of Mexico.

The most widely used $\mathbf{U}^{\mathbf{K}'}_{37}$-SST calibration equation [$\mathbf{U}^{\mathbf{K}'}_{37} = 0.034\,T(°C) + 0.039$] is based on *E. huxleyi* cultured between 8°C and 25°C [*Prahl et al.,* 1988] and has been validated to reflect mean annual SST in global core-top calibration studies [*Müller et al.,* 1998; *Conte et al.,* 2006]. When this equation is applied to the sediment trap time series of $\mathbf{U}^{\mathbf{K}'}_{37}$ data in our study, the $\mathbf{U}^{\mathbf{K}'}_{37}$-SST seasonal amplitude is muted relative to the observed SST range (Figure 4b). $\mathbf{U}^{\mathbf{K}'}_{37}$-SST winter minima are ~2°C warmer than observed SSTs, and summer maxima in $\mathbf{U}^{\mathbf{K}'}_{37}$-SST underestimate observed maxima by ~3°C.

Although our study site covers a narrow temperature (19–30°C) range relative to the global ocean, we calculate the $\mathbf{U}^{\mathbf{K}'}_{37}$-SST relationship in the nGoM sediment trap time series. A second-order polynomial ($r^2 = 0.72$) is the best fit between the $\mathbf{U}^{\mathbf{K}'}_{37}$ and 28 day lagged HadISST data, and a reduced major axis (RMA) linear

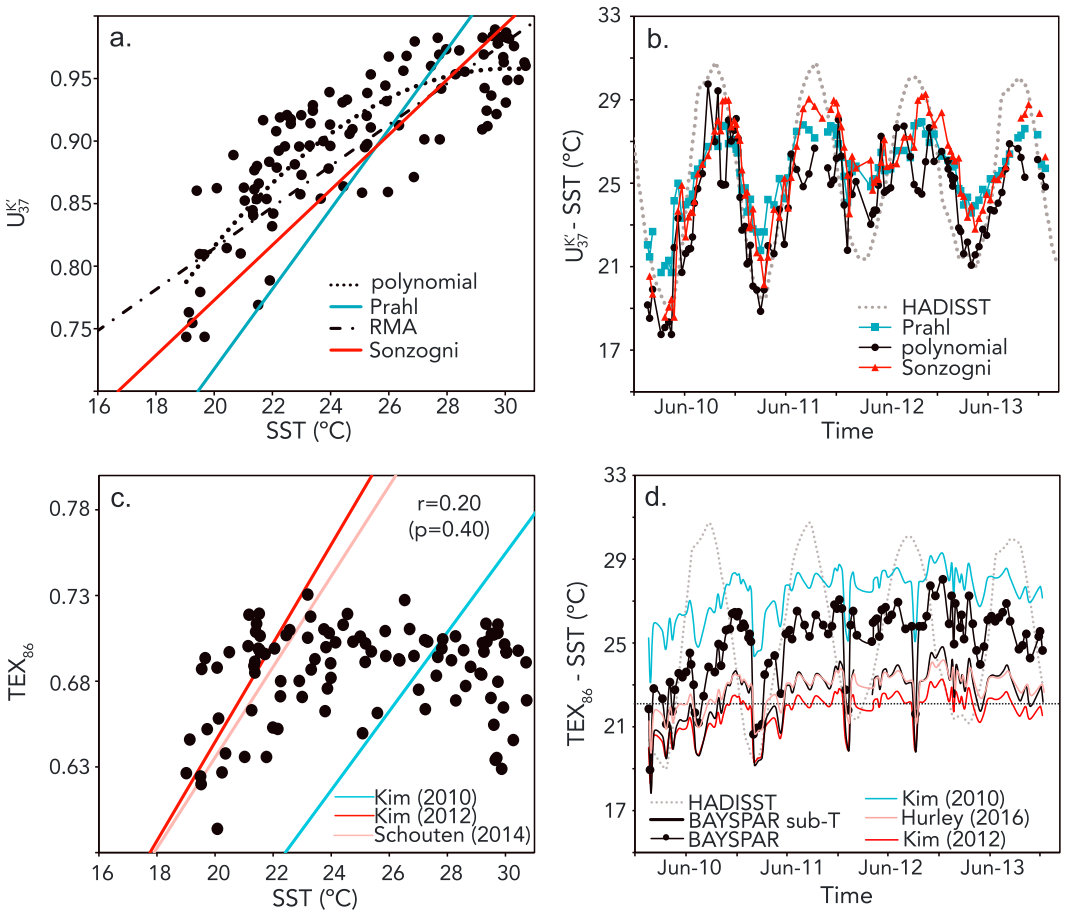

Figure 4. Comparison of different calibration equations for $U^{K'}_{37}$-SST and TEX_{86}-SST. (a) A crossplot of and $U^{K'}_{37}$ from the sediment trap with 28 day lagged HadISST. Published linear $U^{K'}_{37}$-SST calibration lines are shown in red [*Sonzogni et al.*, 1997] and teal [*Prahl et al.*, 1988]. Dashed line shows a polynomial fit, and dash-dotted line shows a reduced major axis (RMA) linear regression for the $U^{K'}_{37}$ of sinking particles and 28 day lagged HadISST. (b) Sediment trap time series of $U^{K'}_{37}$-SST calibrated using the different $U^{K'}_{37}$-SST relationships. The 28 day lagged HadISST is plotted with dashed grey line. (c) A crossplot of TEX_{86} from the sediment trap with HadISST. Published linear TEX_{86}-SST calibration lines are shown in red [*Kim et al.*, 2012], pink [*Schouten et al.*, 2013], and teal [*Kim et al.*, 2010]. (d) Sediment trap time series of TEX_{86}-SST calibrated using the different TEX_{86}-SST relationships from Figure 4c and also the BAYSPAR and BAYSPAR sub-*T* from *Tierney and Tingley* [2015]. HadISST is plotted with dashed grey line, and the climatic mean annual integrated 0–200 m temperature (22.1°C) is indicated by the dashed horizontal line.

regression ($r^2 = 0.66$) between the $U^{K'}_{37}$ and 28 day lagged HadISST data indicates that the slope (0.017 ± 0.001) of the $U^{K'}_{37}$-SST relationship for this data set is much smaller than that of the global equation (0.034) [*Müller et al.*, 1998]. *Sonzogni et al.* [1997] also found the slope of the $U^{K'}_{37}$-SST relationship to be smaller at SSTs above 24°C in an Indian Ocean core-top study. In a study of globally distributed surface ocean (0–30 m) $U^{K'}_{37}$, *Conte et al.* [2006] found that the $U^{K'}_{37}$-SST relationship became nonlinear at SSTs above 26°C. *Conte et al.* [1998] also demonstrated nonlinearity in the $U^{K'}_{37}$-SST relationship at higher temperatures in a culture study using multiple strains of *E. huxleyi* and *G. oceanica*.

When the Sonzogni equation [$U^{K'}_{37} = 0.023$ (°C) + 0.316] is applied to the nGoM data, the residuals between the $U^{K'}_{37}$-SST and the observed SST are smallest, with the $U^{K'}_{37}$-SST accurately reflecting winter minima and underestimating summer SST maxima by 1–2°C. The fact that $U^{K'}_{37}$-SST underestimates the summer SST maxima using all equations may indicate that either $U^{K'}_{37}$ represents deeper alkenone production than the surface mixed layer in summer or that coccolithophores are nutrient stressed, which has been shown to lower $U^{K'}_{37}$ in culture experiments [*Prahl et al.*, 2003]. We consider the former possibility to the most likely explanation,

as it has been observed in the Atlantic that deep production of alkenones below the mixed layer peaks during summer stratification [*Kinkel et al*., 2000]. A coccolithophorid assemblage study in the southwestern Gulf of Mexico likewise indicates that coccolithophorid abundance peaks between 50 and 100 m water depth with *E. huxleyi* dominating the assemblage down to 100 m [*Baumann and Boeckel*, 2013]. The upper water column in the nGoM is highly stratified in the summer, with an integrated temperature of 28–29°C for the upper 75 m of the water column (based on August 2011 and 2012 CTD casts at the site). If we use the Sonzogni equation, it gives us summer maximum $\mathbf{U}^{\mathbf{K}'}_{37}$-temperatures of 29.0 (±0.1)°C, consistent with the alkenones representing an integrated 0–75 m signal.

While the Sonzogni equation yields the best match between $\mathbf{U}^{\mathbf{K}'}_{37}$ in sinking particles and local SST, it may overestimate SST variability when applied to downcore $\mathbf{U}^{\mathbf{K}'}_{37}$ records spanning intervals where mean annual SST transitioned between <24°C and >24°C in the Gulf of Mexico (e.g., the Last Glacial Maximum (LGM) to late Holocene). For example, *Jasper and Gagosian* [1989] published a $\mathbf{U}^{\mathbf{K}'}_{37}$ time series from the Pigmy Basin (Deep Sea Drilling Project site 619, 27° 11.61′N, 91° 24.54′W) with an LGM-to-Holocene $\mathbf{U}^{\mathbf{K}'}_{37}$ range of 0.68–0.86. Applying the *Prahl et al*. [1988] equation to these data yields a 5°C LGM-Holocene warming (19–24°C), while the *Sonzogni et al.* [1997] equation yields a >7°C LGM-Holocene warming (16–23.5°C). Foraminiferal paired Mg/Ca and oxygen isotopes ($\delta^{18}O_c$) from the Orca Basin [*Williams et al.,* 2010] and DeSoto Canyon [*Nürnberg et al.,* 2008] estimate a 5–6°C LGM-Holocene warming in the nGoM (Mg/Ca-$\delta^{18}O_c$ records were recalibrated to SST accounting for the influence of salinity on Mg/Ca, see supporting information). We suggest that the *Prahl et al.* [1988] equation is appropriate for assessing glacial-interglacial $\mathbf{U}^{\mathbf{K}'}_{37}$-SST variability in the nGoM but would likely underestimate SST variability during the Holocene, when mean annual SST in the nGoM varied between 23°C and 27°C.

5. TEX_{86}-SST Estimates

The TEX_{86} of sinking particles (0–700 m) ranges from 0.594 to 0.731 over the 4 year time series, with a flux-weighted mean value of 0.676. TEX_{86} does not covary in a systematic way with overlying SST (Figure 2a). January isoGDGT flux maxima in 2010, 2011, and 2012 are characterized by lowest monthly TEX_{86} values in the time series, but relative lows in TEX_{86} also occur in midsummer of 2010 and 2012. When TEX_{86} is regressed against local HadISST, there is no correlation between a 0 and 28 days lag. The absence of a seasonal cycle and no correlation with contemporaneous surface temperatures suggests that the TEX_{86} signal is likely composed of a mixture of surface and deeper sources of GDGT production. A snapshot of Thaumarchaeota populations in the northern Gulf of Mexico found that they were present throughout the water column with peak abundance was near the base of the oxycline, 100–200 m water depth [*Tolar et al.,* 2013]. Although there are studies in which TEX_{86} in the water column reflects the seasonal cycle in SST [e.g., *Wuchter et al.,* 2006; *Basse et al.,* 2014], our result is consistent with sediment trap time series in the Pacific [*Huguet et al.,* 2007; *Yamamoto et al.,* 2012; *Chen et al.,* 2016], Indian Ocean [*Fallet et al.,* 2011], and Atlantic [*Turich et al.,* 2013; *Mollenhauer et al.,* 2015], where TEX_{86} of sinking particles does not covary with the annual cycle in SST.

Despite the apparent lack of correlation with monthly SST, the TEX_{86} time series does reflect colder conditions in the winter of 2009–2010 and 2010–2011, relative to the latter two winters. This suggests that interannual variability is recorded in TEX_{86}, either due to changes in the relative contribution of surface versus subsurface (0–200 m) GDGT production, or perhaps more likely due to cocorrelation between surface and subsurface temperature variability. Both the TEX_{86} and $\mathbf{U}^{\mathbf{K}'}_{37}$ time series indicate that the winter of 2009–2010 was the coldest in the 4 year sampling interval, coinciding with anomalously cold SST minima recorded in the CTD and HadISST data from the nGoM. The winter of 2009–2010 has the lowest ocean heat content observed in the North Atlantic Ocean during the past decade [*Bryden et al.,* 2014] and coincided with a reduction in Atlantic Meridional Overturning Circulation, a negative North Atlantic Oscillation, and a moderately strong El Niño.

There are a number of published TEX_{86}-SST calibration equations, including global core-top calibration data sets that relate TEX_{86} to surface or integrated shallow subsurface (50–200 m) temperature [*Kim et al.,* 2010, 2012; *Tierney and Tingley,* 2014, 2015], and suspended particulate matter-based calibrations [*Wuchter et al.,* 2004; *Hurley et al.,* 2016]. Applying the BAYSPAR (Bayesian, spatially varying) SST calibration [*Tierney and*

Tingley, 2015] results in a flux-weighted mean of 25.3°C for the 4 year time series, equivalent to the climatic mean annual SST for the northern Gulf of Mexico [*Locarnini et al.,* 2010]. The BAYSPAR sub-*T* calibration results in a flux-weighted mean of 22.0°C, which is nearly equivalent to the integrated 0–200 m mean annual temperature (22.1°C) in the nGoM [*Locarnini et al.,* 2010] . The *Kim et al.* [2012] equation (which calibrated TEX_{86}^{H} to the 0–200 m water temperature in a global core-top data set) applied to this time series results in a flux-weighted mean temperature of 21.4°C, slightly cooler than the 0–200 m integrated temperature, and the *Hurley et al.* [2016] equation generated from sinking particles in the upper 100 m of the water column returns a flux-weighted mean of 22.7°C, which is a reasonable estimate of the integrated 0–100 m mean annual temperature in the nGoM (23.8°C) [from *Locarnini et al.,* 2010] . This strongly suggests that GDGTs in the nGoM derive from the integrated subsurface (0–200 m), which is also consistent with an apparent lack of seasonality.

Using the *Kim et al.* [2010] global core-top calibration of TEX_{86}^{H} to SST results in a flux-weighted mean SST of 26.9°C for this sediment trap data set. This is 1.5°C warmer than the mean annual SST in the nGoM. Since the flux of isoGDGTs is weighted toward the winter and likely integrates a subsurface signal at this location, the *Kim et al.* [2010] equation yields unrealistically high SST estimates in the northern Gulf of Mexico. A downcore TEX_{86} record from the Pigmy Basin in the nGoM was calibrated to SST using the *Kim et al.* [2010] equation and indicated that TEX_{86}-SST was 3°C warmer than foraminiferal Mg/Ca-SST estimates over the past millennium [*Richey et al.,* 2011]. Based on that study, the conclusion was drawn that GDGT flux was summer weighted or confined to the surface mixed layer. The sediment trap data do not support that conclusion but rather suggest that TEX_{86} represents mean annual shallow subsurface temperatures. However, when the downcore Pigmy Basin TEX_{86} record is recalibrated using the BAYSPAR SST calibration, it shows a consistent range and pattern of SST variability consistent with the Mg/Ca-SST record [*Richey et al.,* 2007] This suggests that in spite of subsurface production, the TEX_{86} can still be used to infer SSTs reliably on decadal and longer timescales (see supporting information Figure S3).

Indices such as Methane Index (MI) and the Ring Index (RI) have been developed to make additional inferences from the degree of cyclization in isoGDGTs 0-V. *Zhang et al.* [2011] found that MI values above 0.3 may indicate the contribution of GDGTs from methanotrophic archaea, which could overprint on the thermally derived TEX_{86} signal. The mean MI values of 0.24 ($\pm$0.02) in nGoM sinking particles and 0.22 ($\pm$0.01) in nGoM sediments are within the range of typical values for pelagic marine sediments, so significant influence of methanogenesis on TEX_{86} at our study site is unlikely. It has been observed in cultures of thaumarchaeota [*Qin et al.,* 2015] and in thermophilic archaea [*Pearson et al.,* 2004] that RI varies more systematically as a function of temperature than TEX_{86} does. In the global core-top data set, both TEX_{86} and RI increase with increasing SST, and *Zhang et al.* [2015] suggest that deviations from the global TEX_{86}-RI relationship may be used to indicate nontemperature influences on the TEX_{86} proxy.

We find no correlation between SST and TEX_{86} ($r = 0.20$, $p = 0.40$) or SST and RI ($r = -0.14$, $p = 0.72$) in sinking particles. However, the positive correlation ($r = 0.5$; $p < 0.02$) between TEX_{86} and RI at our sediment trap site (Figure 5a) suggests a common thermal control on both. With the exception of two samples, the difference between measured and predicted RI ($|\Delta RI|$) is always <0.3 and thus within the 95% confidence interval of the global regression. One interesting observation in the sediment trap time series is that the RI of sinking particles in the nGoM is always slightly higher than the RI_{TEX} predicted by the global TEX_{86}-RI relationship (i.e., $\Delta RI < 0$) in *Zhang et al.* [2015]. This result was also observed by *Zhang et al.* [2015] in a Mediterranean core-top data set of shallow water ($<$1000 m) sites [*Kim et al.,* 2015]. Additionally, the ΔRI becomes increasingly negative with decreasing TEX_{86} (Figure 5c) and increasing TOC flux (Figure 5d) in sinking particles. One potential explanation for this relationship may be a change in the relative abundance of heterotrophic versus autotrophic archaea in response to changing availability of OC (via particulate organic carbon (POC) flux) for heterotrophic consumption. If heterotrophic archaea produce GDGTs with a larger RI value than their autotrophic counterparts, then it is possible that relative increases in their production would lead to the observed pattern. Likewise, oceanographic environments with relatively high fluxes of POC, such as shallow sites near the continental margins, may display a ΔRI that is similarly offset from the global mean. A survey of water column community structure in the nGoM showed that the abundance of heterotrophic Euryarchaeota relative to Thaumarchaeota was much larger in near-surface (upper 100 m) water column for sites impacted by the Mississippi plume. Thaumarchaeota dominated at all depths $>$100 m [*Tolar et al.,* 2013].

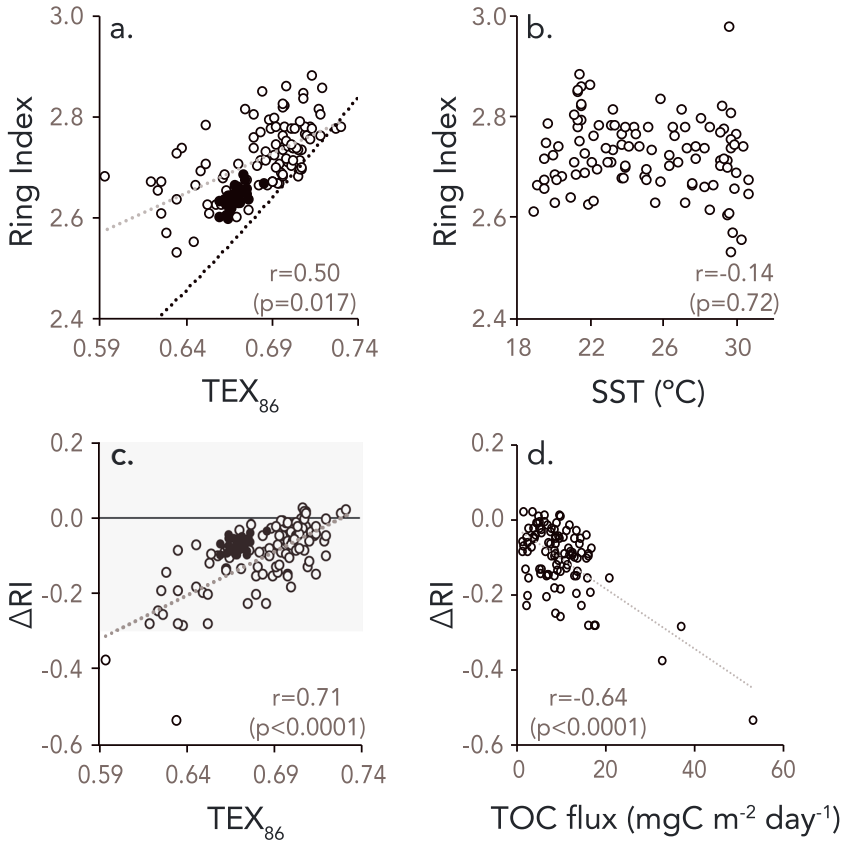

Figure 5. Ring Index (RI) in sinking particles (open circles) and core-top (solid circles) samples in the northern Gulf of Mexico. (a) RI plotted as a function of TEX_{86}. Black dashed curve shows the relationship between TEX_{86} and RI for the global core-top data set determined by *Zhang et al.* [2015], while the grey dashed line is the relationship in this data set. (b) Plot of RI versus SST in sinking particles. (c) ΔRI versus TEX_{86}, where ΔRI is the difference between the measured RI and the RI predicted by TEX_{86} using the equation of *Zhang et al.* [2015]. (d) ΔRI versus corresponding total organic carbon (TOC) flux in sinking particles.

6. Comparison of Sinking Particles to Underlying Sediments

6.1. Alkenones

We compared the $U^{K'}_{37}$-SST of sediments from three multicores recovered at the sediment trap site (1150 m water depth) to that of sinking particles from the overlying water column. $U^{K'}_{37}$ analyses of 10 samples from the upper 5 cm of 3 independent multicores (~60 years of sedimentation) were conducted. The mean $U^{K'}_{37}$ for the upper 5 cm of sediment is 0.92 (±0.01), which is significantly higher than the flux-weighted mean $U^{K'}_{37}$ of 0.88 (±0.01) from sinking particles in the overlying water column. This results in a warm bias of 1.3–2.4°C in sedimentary $U^{K'}_{37}$-SST, depending on the calibration equation used (Table 1). This warm bias in sediments relative to sinking particles is not typical for the global distribution of water column-sediment comparisons [*Rosell-Melé and Prahl*, 2013], but has been observed in other studies [*Hoefs et al.,* 1998; *Gong and Hollander*, 1999], and may indicate preferential diagenetic loss of $C_{37:3}$ in nGoM sediments. Culture studies have demonstrated that selective degradation $C_{37:3}$ alkenone by certain strains of aerobic heterotropic bacteria lead to increases in the $U^{K'}_{37}$ equivalent to 1–3°C [*Rontani et al.,* 2008; *Zabeti et al.,* 2010]. Autoxidation of alkenones throughout the water column and in aerobic sediments can also cause selectively degrade $C_{37:3}$ alkenone, effectively leading to anomalously warm $U^{K'}_{37}$-SST estimates [*Rontani et al.*, 2006]. *Prahl et al.* [2003] observed that *E. huxleyi* cells selectively catabolized $C_{37:3}$ alkenone under extreme light limitation, which could also lead to $U^{K'}_{37}$-SST estimates that are up to 3°C warmer than expected. This is not likely to be the cause for the warm bias in sedimentary alkenones versus sinking particles in this study, as we do not see a warm bias in sinking particles collected at 700 m depth. Since alkenone flux is winter weighted in the

Table 1. Comparison of the Flux-Weighted Mean (From Sinking Particles) and Core-Top TEX_{86}-SST and $U^{K'}_{37}$-SST, Calibrated Using the Various Calibration Equations[a]

Calibration	Flux-Weighted Mean TEX_{86}	Flux-Weighted Mean $U^{K'}_{37}$	Mean Core Top (0–5 cm) TEX_{86}	Mean Core Top (0–5 cm) $U^{K'}_{37}$
	0.676 (±0.001)	0.88 (±0.01)	0.670 (±0.006)	0.92 (±0.01)
BAYSPAR	25.3°C	—	24.9 (±0.4)°C	—
BAYSPAR sub-*T*	22.0°C	—	21.7 (±0.3)°C	—
Kim et al. [2010]	27.0°C	—	26.7 (±0.3)°C	—
Kim et al. [2012]	21.4°C	—	21.2 (±0.2)°C	—
Hurley et al. [2016]	22.7°C	—	21.6 (±0.2)°C	—
Prahl et al. [1988]	—	24.8°C	—	26.1 (±0.3)°C
Sonzogni et al. [1997]	—	24.6°C	—	25.8 (±0.4)°C

[a]Errors presented for the mean core-top TEX_{86}-SST and $U^{K'}_{37}$-SST represent the standard deviation of all measurements in the upper 5 cm of sediment from all three subcores.

nGoM, and summer alkenone production may include a subsurface signal, diagenetic loss of $C_{37:3}$ is the most likely explanation for warmer than predicted $U^{K'}_{37}$ values in sediments. It is possible that this phenomenon varies within the nGoM as a function water depth, sediment accumulation rate, and redox conditions at the sediment-water interface.

6.2. GDGTs

The mean TEX_{86} value for the upper 5 cm of sediment from three multicores is 0.670 (±0.006). This is not significantly different from the flux-weighted mean TEX_{86} value of 0.676 (±0.001) for sinking particles in the 4 year sediment trap time series, suggesting that TEX_{86} in sediments represents a local, unaltered representation of planktonic GDGT production in the water column. The BIT index is an order of magnitude higher in sediments (mean BIT = 0.13 ± 0.04) than in sinking particles, indicating that the majority of terrestrially derived brGDGTs are being delivered via lateral transport from the shelf to the slope but also that terrestrially derived GDGTs are not influencing the TEX_{86} signal.

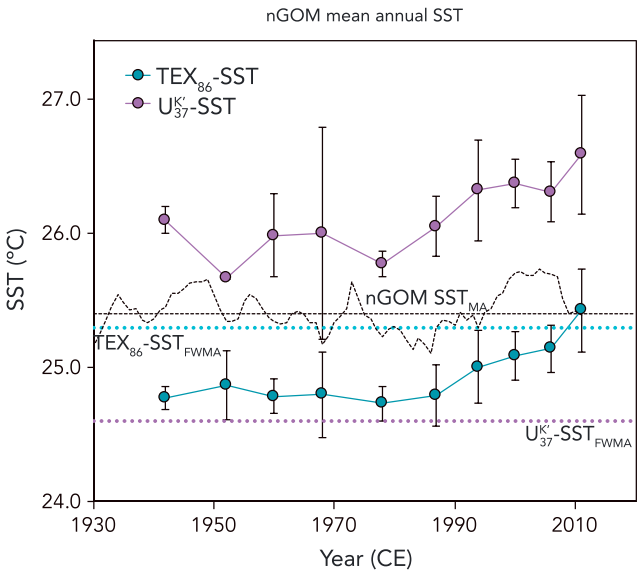

Figure 6. Downcore TEX_{86}-SST and $U^{K'}_{37}$-SST data from the upper 5 cm of northern Gulf of Mexico multicores. Each data point represents the mean of three samples from the same depth horizon in three different multicores collected from the sediment trap site (1150 m water depth), and error bars indicate the standard deviation among those three multicores. The age model is based on a ^{210}Pb chronology developed from a fourth multicore. $U^{K'}_{37}$ is converted to SST using the *Sonzogni et al.* [1997] equation, and TEX_{86} is calibrated to SST using BAYSPAR [*Tierney and Tingley*, 2015]. The black dashed time series is the mean annual HadISST (3 year running mean) for the nGoM. The purple and teal dashed lines represent the flux-weighted mean annual $U^{K'}_{37}$ and TEX_{86}-SSTs, respectively, based on the 4 year sediment trap time series in this study.

7. Proxy Comparison

A comparison of $U^{K'}_{37}$-SST and TEX_{86}-SST in co-occurring sediments from the past century shows offsets in the absolute SST estimates of the two proxies, but both show nearly identical trends in surface ocean warming over the past three decades (Figure 6). The downcore $U^{K'}_{37}$ and TEX_{86} data were calibrated to SST using the *Sonzogni et al.* [1997] and BAYSPAR SST [*Tierney and Tingley*, 2015] equations, respectively. High sediment accumulation rates (58 cm/kyr) in the northern Gulf of Mexico allow us to resolve the SST signal for the past century—the TEX_{86} and $U^{K'}_{37}$ in the upper 5 cm of the sediments both indicate a warming trend of 0.02°C yr^{-1}, or 0.8 (±0.2)°C of warming since 1975 Common Era (C.E.). HadISST data from nearest to the core site do not show consistent warming across the twentieth century but do show a warming of

0.5°C since 1975 that is in general agreement with the magnitude recorded by the proxies (Figure 6). Despite spatial and temporal uncertainties inherent to comparing three separate subcores, the warming trend is present in the individual time series of both proxies from all three cores. It should be noted as well that bioturbation is expected to smear the signal in the multicores; thus, we do not expect to recover subdecadal features in the biomarker data. Nonetheless, the multicore data demonstrate that both proxies are capable of recording surface temperature conditions. In the case of TEX_{86}, this indicates that surface temperature inference is possible because on interannual and longer timescales, subsurface and surface temperatures covary.

8. Conclusions

A 4 year time series of the TEX_{86} and $\mathbf{U}^{\mathbf{K}'}_{37}$ variations in sinking particles from a nGoM sediment trap reveals that both biomarker proxies export a signal to marine sediments reflects upper ocean mean annual temperatures. $\mathbf{U}^{\mathbf{K}'}_{37}$ covaries with the seasonal cycle in SST and the $\mathbf{U}^{\mathbf{K}'}_{37}$-SST at the nGoM sediment trap site reveals a smaller slope than the global $\mathbf{U}^{\mathbf{K}'}_{37}$-SST relationship, indicating nonlinearity in the high SST range (24–30°C). TEX_{86} in sinking particles displays no systematic relationship to SST on a subannual timescale but does reflect interannual variability in mean annual SST. We conclude that this can be attributed to cocorrelation between surface temperatures and subsurface (0–200 m) temperatures on the interannual timescale. Downcore TEX_{86} measurements in the nGoM confirm that TEX_{86} can be used to reconstruct SSTs in spite of integrating subsurface temperatures and thus that TEX_{86} can be used to infer either subsurface or surface temperatures in the nGoM reliably.

Core-top TEX_{86} is within analytical uncertainty of the flux-weighted mean estimate from sinking particles in the overlying water column, indicating that local autochthonous GDGT production is the primary source of isoprenoid GDGTs in the nGoM sediments and that the TEX_{86} of sedimentary GDGTs is not altered by diagenesis. The flux-weighted mean $\mathbf{U}^{\mathbf{K}'}_{37}$ of sinking particles is significantly lower than that of underlying sediments, suggesting preferential diagenetic loss of $C_{37:3}$ alkenone at the sediment-water interface. This leads to a 1–2°C warm bias in sedimentary alkenone-based SST estimates at this site.

In summary, $\mathbf{U}^{\mathbf{K}'}_{37}$ signal exported to the sediment reflects near-surface, mean annual temperature in the northern Gulf of Mexico. Care should be taken when choosing a $\mathbf{U}^{\mathbf{K}'}_{37}$-SST calibration, due to the observed nonlinearity in the relationship at the high end of the SST range in the nGoM. We recommend the *Sonzogni et al.* [1997] equation for recent (modern-to-late Holocene) records. TEX_{86}, on the other hand, reflects an integrated mean annual subsurface (0–200 m) temperature in the northern Gulf of Mexico, indicating that the BAYSPAR sub-*T* calibration is the most suitable for converting TEX_{86} to temperature. However, when TEX_{86} is converted to temperature using the BAYSPAR SST calibration, it shows a similar pattern and magnitude of temperature change over the past century as $\mathbf{U}^{\mathbf{K}'}_{37}$, with nearly identical rates of surface ocean warming in the nGoM since 1975 C.E. This, combined with evidence from the 1000 year Pigmy Basin TEX_{86} record (*Richey et al.* [2011] and see supporting information), suggests that TEX_{86} can be used to infer SSTs in the nGoM in spite of subsurface production, most likely because SSTs and subsurface temperatures covary over these timescales.

Acknowledgments
We thank Eric Tappa, Caitlin Reynolds, Kaustubh Thirumalai, and the LUMCON crew of the R/V *Pelican* for ongoing maintenance of the sediment trap mooring. Thanks to Cole Spencer and Tess Busch for laboratory preparation of samples for geochemical analysis. Chris Smith and Marci Marot conducted ^{210}Pb analyses for multicore chronology at the USGS, St. Petersburg Coastal and Marine Science Center. We thank K. Thirumalai and two anonymous reviewers for their constructive comments on this manuscript. This research was supported by the USGS Climate and Land Use Research and Development Program. Any use of trade, firm, or product names is for descriptive purposes only and does not imply endorsement by the U.S. Government. All new data presented in this study can be accessed in the USGS Data Release [*Richey and Tierney*, 2016], F76M350W.

References

Balmaseda, M. A., K. Mogensen, and A. T. Weaver (2012), Evaluation of the ECMWF ocean reanalysis system ORAS4, *Q. J. R. Meteorol. Soc.*, *139*, 1132–1161.

Basse, A., C. Zhu, G. J. M. Versteegh, G. Fischer, K.-U. Hinrichs, and G. Mollenhauer (2014), Distribution of intact and core tetraether lipids in water column profiles of suspended particulate matter off Cape Blanc, NW Africa, *Org. Geochem.*, *72*, 1–13.

Baumann, K. H., and B. Boeckel (2013), Spatial distribution of living coccolithophores in the southwestern Gulf of Mexico, *J. Micropalaeontol.*, *32*(2), 123–133.

Brassell, S. C. (1993), Applications of biomarkers for delineating marine palae-oclimatic fluctuations during the Pleistocene, in *Organic Geochemistry Principles and Applications*, edited by M. H. Engel and S. A. Macko, pp. 699–738, Plenum, New York.

Brassell, S. C., G. Eglinton, I. T. Marlowe, U. Pflaumann, and M. Sarnthein (1986), Molecular stratigraphy: A new tool for climatic assessment, *Nature*, *320*, 129–133.

Bryden, H. L., B. A. King, G. D. McCarthy, and E. L. McDonagh (2014), Impact of a 30% reduction in Atlantic meridional overturning during 2009–2010, *Ocean Sci.*, *10*(4), 683–691.

Castañeda, I. S., E. Schefuß, J. Pätzold, J. S. Sinninghe Damsté, S. Weldeab, and S. Schouten (2010), Millennial-scale sea surface temperature changes in the eastern Mediterranean (Nile River Delta region) over the last 27,000 years, *Paleoceanography*, *25*, PA1208, doi:10.1029/2009PA001740.

Chen, W., M. Mohtadi, E. Schefuß, and G. Mollenhauer (2016), Concentrations and abundance ratios of long-chain alkenones and glycerol dialkyl glycerol tetraethers in sinking particles south of Java, *Deep Sea Res., Part I*, *112*, 14–24.

Conte, M. H., G. Eglinton, and L. A. S. Madureira (1992), Long-chain alkenones and alkyl alkenoates as palaeotemperature indicators: Their production, flux and early sedimentary diagenesis in the Eastern North Atlantic, *Org. Geochem.*, *19*, 287–298.

Conte, M. H., A. Thompson, D. Lesley, and R. P. Harris (1998), Genetic and physiological influences on the alkenone/alkenoate versis growth temperature relationship in *Emiliania huxleyi* and *Gephyrocapsa oceanica*, *Geochim. Cosmochim. Acta*, *62*, 51–68.

Conte, M. H., M.-A. Sicre, C. Rühlemann, J. C. Weber, S. Schulte, D. Schulz-Bull, and T. Blanz (2006), Global temperature calibration of the alkenone unsaturation index ($U^{K'}_{37}$) in surface waters and comparison with surface sediments, *Geochem. Geophys. Geosyst.*, *7*, Q02005, doi:10.1029/2005GC001054.

Damsté, J. S. S., S. Schouten, E. C. Hopmans, A. C. van Duin, and J. A. Geenevasen (2002), Crenarchaeol the characteristic core glycerol dibiphytanyl glycerol tetraether membrane lipid of cosmopolitan pelagic crenarchaeota, *J. Lipid Res.*, *43*(10), 1641–1651.

D'souza, N. A., A. Subramaniam, A. R. Juhl, M. Hafez, A. Chekalyuk, S. Phan, B. Yan, I. R. MacDonald, S. C. Weber, and J. P. Montoya (2016), Elevated surface chlorophyll associated with natural oil seeps in the Gulf of Mexico, *Nat. Geosci.*, *9*(3), 215–218.

Ebisuzaki, W. (1997), A method to estimate the statistical significance of a correlation when the data are serially correlated, *J. Clim.*, *10*(9), 2147–2153.

Epstein, B. L., S. D'Hondt, J. G. Quinn, J. Zhang, and P. E. Hargraves (1998), An effect of dissolved nutrient concentration on alkenone-based temperature estimates, *Paleoceanogr. Curr.*, *13*(2), 122–126.

Epstein, B. L., S. D'Hondt, and P. E. Hargraves (2001), The possible metabolic role of C_{37} alkenones in *Emiliania huxleyi*, *Org. Geochem.*, *32*, 867–875.

Fallet, U., J. E. Ullgren, I. S. Castañeda, H. M. van Aken, S. Schouten, H. Ridderinkhof, and G.-J. A. Brummer (2011), Contrasting variability in foraminiferal and organic paleotemperature proxies in sedimenting particles of the Mozambique Channel (SW Indian Ocean), *Geochim. Cosmochim. Acta*, *75*(20), 5834–5848.

Fischer, G., and G. Karakas (2009), Sinking rates and ballast composition of particles in the Atlantic Ocean: Implications for the organic carbon fluxes to the deep ocean, *Biogeosciences*, *6*, 85–102.

Gong, C., and D. J. Hollander (1999), Evidence for differential degradation of alkenones under contrasting bottom water oxygen conditions: Implication for paleotemperature reconstruction, *Geochim. Cosmochim. Acta*, *63*, 405–411.

Hoefs, M. J. L., G. J. M. Versteegh, W. I. C. Rijpstra, J. W. deLeeuw, and J. S. S. Damsté (1998), Postdepositional oxic degradation of alkenones: Implications for the measurement of palaeo sea surface temperatures, *Paleoceanography*, *13*, 42–49, doi:10.1029/97PA02893.

Hopmans, E. C., J. W. H. Weijers, E. Schefuß, L. Herfort, J. S. Sinninghe Damsté, and S. Schouten (2004), A novel proxy for terrestrial organic matter in sediments based on branched and isoprenoid tetraether lipids, *Earth Planet. Sci. Lett.*, *224*(1–2), 107–116.

Huang, H., N. D. Walker, Y. Hsueh, Y. Chao, and R. R. Leben (2013), An analysis of Loop Current frontal eddies in a 1/6° Atlantic ocean model simulation, *J. Phys. Oceanogr.*, *43*(9), 1924–1939.

Huguet, C., J.-H. Kim, J. S. Sinninghe Damsté, and S. Schouten (2006), Reconstruction of sea surface temperature variations in the Arabian Sea over the last 23 kyr using organic proxies (TEX_{86} and $U_{37}^{K'}$), *Paleoceanography*, *21*, PA3003, doi:10.1029/2005PA001215.

Huguet, C., A. Schimmelmann, R. Thunell, L. J. Lourens, J. S. Sinninghe Damsté, and S. Schouten (2007), A study of the TEX_{86} paleothermometer in the water column and sediments of the Santa Barbara Basin, California, *Paleoceanography*, *22*, PA3203, doi:10.1029/2006PA001310.

Hurley, S. J., F. J. Elling, M. Könneke, C. Buchwald, S. D. Wankel, A. E. Santoro, J. S. Lipp, K.-U. Hinrichs, and A. Pearson (2016), Influence of ammonia oxidation rate on thaumarchaeal lipid composition and the TEX_{86} temperature proxy, *Proc. Natl. Acad. Sci. U.S.A.*, *113*(28), 7762–7767.

Jasper, J. P., and R. B. Gagosian (1989), Alkenone molecular stratigraphy in an oceanic environment affected by glacial freshwater events, *Paleoceanography*, *4*, 603–614, doi:10.1029/PA004i006p00603.

Kim, J.-H., J. van der Meer, S. Schouten, P. Helmke, V. Willmott, F. Sangiorgi, N. Koç, E. C. Hopmans, and J. S. S. Damsté (2010), New indices and calibrations derived from the distribution of crenarchaeal isoprenoid tetraether lipids: Implications for past sea surface temperature reconstructions, *Geochim. Cosmochim. Acta*, *74*(16), 4639–4654.

Kim, J.-H., O. E. Romero, G. Lohmann, B. Donner, T. Laepple, E. Haam, and J. S. Sinninghe Damsté (2012), Pronounced subsurface cooling of North Atlantic waters off Northwest Africa during Dansgaard–Oeschger interstadials, *Earth Planet. Sci. Lett.*, *339–340*, 95–102.

Kim, J.-H., et al. (2015), Influence of deep-water derived isoprenoid tetraether lipids on the TEX_{86} paleothermometer in the Mediterranean Sea, *Geochim. Cosmochim. Acta*, *150*, 125–141.

Kourafalou, V. H., and Y. S. Androulidakis (2013), Influence of Mississippi River induced circulation on the Deepwater Horizon oil spill transport, *J. Geophys. Res. Oceans*, *118*, 3823–3842, doi:10.1002/jgrc.20272.

Leduc, G., R. Schneider, J. H. Kim, and G. Lohmann (2010), Holocene and Eemian sea surface temperature trends as revealed by alkenone and Mg/Ca paleothermometry, *Quat. Sci. Rev.*, *29*, 989–1004, doi:10.1016/j.quascirev.2010.01.004.

Lincoln, S. A., B. Wai, J. M. Eppley, M. J. Church, R. E. Summons, and E. F. DeLong (2014), Planktonic Euryarchaeota are a significant source of archaeal tetraether lipids in the ocean, *Proc. Natl. Acad. Sci. U.S.A.*, *111*(27), 9858–9863.

Lipp, J. S., Y. Morono, F. Inagaki, and K. U. Hinrichs (2008), Significant contribution of Archaea to extant biomass in marine subsurface sediments, *Nature*, *454*(7207), 991–994.

Liu, Z., M. Pagani, D. Zinniker, R. DeCanto, M. Huber, H. Brinkhuis, S. R. Shah, R. M. Leckie, and A. Pearson (2009), Global cooling during the Eocene-Oligocene Climate transition, *Science*, *323*, 1187–1190.

Locarnini, R. A., A. V. Mishonov, J. I. Antonov, T. P. Boyer, H. E. Garcia, O. K. Baranova, M. M. Zweng, and D. R. Johnson (2010), *World Ocean Atlas 2009*, vol. 1, *Temp., NOAA Atlas NESDIS 68*, edited by S. Levitus, 184 pp., U.S. Gov. Print. Off., Washington, D. C. [Available at http://www.nodc.noaa.gov/OC5/WOD09/pr_wod09.html.]

Martínez-Garcia, A., A. Rosell-Melé, W. Geibert, R. Gersonde, P. Masque, V. Gaspari, and C. Barbante (2009), Links between iron supply, marine productivity, sea surface temperature, and CO_2 over the last 1.1 Ma, *Paleoceanography*, *24*, PA1207, doi:10.1029/2008PA001657.

Mollenhauer, G., T. I. Eglinton, E. C. Hopmans, and J. S. Sinninghe Damsté (2008), A radiocarbon-based assessment of the preservation characteristics of crenarchaeol and alkenones from continental margin sediments, *Org. Geochem.*, *39*(8), 1039–1045, doi:10.1016/j.orggeochem.2008.02.006.

Mollenhauer, G., A. Basse, J.-H. Kim, J. S. Sinninghe Damsté, and G. Fischer (2015), A four-year record of $U^{K'}_{37}$- and TEX_{86}-derived sea surface temperature estimates from sinking particles in the filamentous upwelling region off Cape Blanc, Mauritania, *Deep Sea Res., Part I*, *97*, 67–79.

Müller, P. J., and G. Fischer (2001), A 4-year sediment trap record of alkenones from the filamentous upwelling region off Cape Blanc, NW Africa and a comparison with distributions in underlying sediments, *Deep Sea Res., Part I*, *48*, 1877–1903.

Müller, P. J., G. Kirst, G. Ruhland, I. von Storch, and A. Rosell-Melé (1998), Calibration of the alkenone paleotemperature index $U^{K'}_{37}$ based on core-tops from the eastern South Atlantic and the global ocean (60°N–60°S), *Geochim. Cosmochim. Acta*, *62*, 1757–1772.

Muller-Karger, F. E., et al. (2015), Natural variability of surface oceanographic conditions in the offshore Gulf of Mexico, *Prog. Oceanogr.*, *134*, 54–76.
Nürnberg, D., M. Ziegler, C. Karas, R. Tiedemann, and M. W. Schmidt (2008), Interacting Loop Current variability and Mississippi River discharge over the past 400 kyr, *Earth Planet. Sci. Lett.*, *272*(1–2), 278–289.
Pearson, A., Z. Huang, A. E. Ingalls, C. S. Romanek, J. Wiegel, K. H. Freeman, R. H. Smittenberg, and C. L. Zhang (2004), Nonmarine Crenarchaeol in Nevada Hot Springs, *Appl. Environ. Microbiol.*, *70*(9), 5229–5237.
Prahl, F. G., L. A. Muehlhausen, and D. L. Zahnle (1988), Further evaluation of long-chain alkenones as indicators of paleoceanographic conditions, *Geochim. Cosmochim. Acta*, *52*, 2303–2310.
Prahl, F. G., M. A. Sparrow, and G. V. Wolfe (2003), Physiological impacts on alkenone paleothermometry, *Paleoceanography*, *18*(2), 1025, doi:10.1029/2002PA000803.
Qin, W., L. T. Carlson, E. V. Armbrust, A. H. Devol, J. W. Moffett, D. A. Stahl, and A. E. Ingalls (2015), Confounding effects of oxygen and temperature on the TEX_{86} signature of marine Thaumarchaeota, *Proc. Natl. Acad. Sci. U.S.A.*, *112*(35), 10,979–10,984.
Rayner, N. A., D. E. Parker, E. B. Horton, C. K. Folland, L. V. Alexander, D. P. Rowell, E. C. Kent, and A. Kaplan (2003), Global analyses of sea surface temperature, sea ice, and night marine air temperature since the late nineteenth century, *J. Geophys. Res., 108*(D14), 4407, doi:10.1029/2002JD002670.
Reynolds, C. E., and J. N. Richey (2016), Seasonal flux and assemblage composition of planktic foraminifera from the northern Gulf of Mexico, 2008–14, *U.S. Geol. Surv. Open–File Rep. 2016-1115*, 19 pp., doi:10.3133/ofr20161115.
Richey, J. N., R. Z. Poore, B. P. Flower, and T. M. Quinn (2007), 1400 yr multiproxy record of climate variability from the northern Gulf of Mexico, *Geology*, *35*(5), 423.
Richey, J. N., D. J. Hollander, B. P. Flower, and T. I. Eglinton (2011), Merging late Holocene molecular organic and foraminiferal-based geochemical records of sea surface temperature in the Gulf of Mexico, *Paleoceanography*, *26*, PA1209, doi:10.1029/2010PA002000.
Richey, J. N., and J. E. Tierney, 2016, GDGT and alkenone flux in the northern Gulf of Mexico, U.S. Geol. Surv. data release, doi:10.5066/F76M350W.
Richey, J. N., C. E. Reynolds, E. Tappa, and R. Thunell (2014), Weekly resolution particulate flux from a sediment trap in the northern Gulf of Mexico, 2008–2012, *U.S. Geol. Surv. Open-File Rep. 2014-1035*, iv, pp. 9.
Rommerskirchen, F., T. Condon, G. Mollenhauer, L. Dupont, and E. Schefuss (2011), Miocene to Pliocene development of surface and subsurface temperatures in the Benguela Current system, *Paleoceanography*, *26*, PA3216, doi:10.1029/2010PA002074.
Rontani, J.-F., J.-C. Marty, J.-C. Miquel, and J. K. Volkman (2006), Free radical oxidation (autoxidation) of alkenones and other microalgal lipids in seawater, *Org. Geochem.*, *37*(3), 354–368.
Rontani, J.-F., R. Harji, S. Guasco, F. G. Prahl, J. K. Volkman, N. B. Bhosle, and P. Bonin (2008), Degradation of alkenones by aerobic heterotrophic bacteria: Selective or not?, *Org. Geochem.*, *39*(1), 34–51.
Rosell-Melé, A., and F. G. Prahl (2013), Seasonality of temperature estimates as inferred from sediment trap data, *Quat. Sci. Rev.*, *72*, 128–136.
Schneider, B., G. Leduc, and W. Park (2010), Disentangling seasonal signals in Holocene climate trends by satellite-model-proxy integration, *Paleoceanography*, *25*, PA4217, doi:10.1029/2009PA001893.
Schouten, S., C. Huguet, E. C. Hopmans, and J. S. Sinninghe Damsté (2007), Analytical methodology for TEX_{86} paleothermometry by high-performance liquid chromatography/atmospheric pressure chemical onization-mass spectrometry, *Anal. Chem.*, *79*, 2940–2944, doi:10.1021/ac062339v.
Schouten, S., A. Pitcher, E. C. Hopmans, L. Villanueva, J. van Bleijswijk, and J. S. S. Damsté (2012), Intact polar and core glycerol dibiphytanyl glycerol tetraether lipids in the Arabian Sea oxygen minimum zone: I. Selective preservation and degradation in the water column and consequences for the TEX_{86}, *Geochim. Cosmochim. Acta*, *98*, 228–243.
Schouten, S., E. C. Hopmans, and J. S. Sinninghe Damsté (2013), The organic geochemistry of glycerol dialkyl glycerol tetraether lipids: A review, *Org. Geochem.*, *54*, 19–61.
Seki, O., D. N. Schmidt, S. Schouten, E. C. Hopmans, J. S. Sinninghe Damsté, and R. D. Pancost (2012), Paleoceanographic changes in the eastern equatorial Pacific over the last 10 Myr, *Paleoceanography*, *27*, PA3224, doi:10.1029/2011PA002158.
Shi, W., and M. Wang (2009), Satellite observations of flood-driven Mississippi River plume in the spring of 2008, *Geophys. Res. Lett.*, *36*, L07607, doi:10.1029/2009GL037210.
Sikes, E. L., W. R. Howard, H. L. Neil, and J. K. Volkman (2002), Glacial-interglacial sea surface temperature changes across the subtropical front east of New Zealand based on alkenone unsaturation ratios and foraminiferal assemblages, *Paleoceanography*, *17*(2), 1012, doi:10.1029/2001PA000640.
Sonzogni, C., E. Bard, F. Rostek, R. Lafont, A. Rodell-Melé, and G. Eglinton (1997), Core-top calibration of the alkenone index vs sea surface temperature in the Indian Ocean, *Deep Sea Res., Part II*, *44*, 1445–1460.
Tierney, J. E., and M. P. Tingley (2014), A Bayesian, spatially-varying calibration model for the TEX_{86} proxy, *Geochim. Cosmochim. Acta*, *127*, 83–106.
Tierney, J. E., and M. P. Tingley (2015), A TEX_{86} surface sediment database and extended Bayesian calibration, *Sci. Data*, *2*, 150029, doi:10.1038/sdata.2015.29.
Tierney, J. E., F. S. R. Pausata, and P. B. deMenocal (2016), Deglacial Indian monsoon failure and North Atlantic stadials linked by Indian Ocean surface cooling, *Nat. Geosci.*, *9*(1), 46–50.
Tolar, B. B., G. M. King, and J. T. Hollibaugh (2013), An analysis of thaumarchaeota populations from the northern Gulf of Mexico, *Front Microbiol.*, *4*, 72.
Turich, C., S. Schouten, R. C. Thunell, R. Varela, Y. Astor, and S. G. Wakeham (2013), Comparison of TEX_{86} and temperature proxies in sinking particles in the Cariaco Basin, *Deep Sea Res., Part I*, *78*, 115–133.
Vukovich, F. M. (1995), An updated evaluation of the Loop Current's eddy-shedding frequency, *J. Geophys. Res.*, *100*, 8655–8659, doi:10.1029/95JC00141.
Walker, N. D., et al. (2011), Impacts of a Loop Current frontal eddy cyclone and wind forcing on the 2010 Gulf of Mexico oil spill, in *Monitoring and Modeling the Deepwater Horizon Oil Spill: A Record-Breaking Enterprise*, *Geophys. Monogr.*, vol. 195, pp. 103–116, AGU, Washington, D. C.
Wang, C., S.-K. Lee, and D. B. Enfield (2008), Atlantic Warm Pool acting as a link between Atlantic Multidecadal Oscillation and Atlantic tropical cyclone activity, *Geochem. Geophys. Geosyst.*, *9*, Q05V03, doi:10.1029/2007GC001809.
Williams, C., B. P. Flower, D. W. Hastings, T. P. Guilderson, K. A. Quinn, and E. A. Goddard (2010), Deglacial abrupt climate change in the Atlantic Warm Pool: A Gulf of Mexico perspective, *Paleoceanography*, *25*, PA4221, doi:10.1029/2010PA001928.
Wuchter, C., S. Schouten, M. J. L. Coolen, and J. S. Sinninghe Damsté (2004), Temperature-dependent variation in the distribution of tetraether membrane lipids of marine Crenarchaeota: Implications for TEX_{86} paleothermometry, *Paleoceanography*, *19*, PA4028, doi:10.1029/2004PA001041.

Wuchter, C., S. Schouten, S. G. Wakeham, and J. S. Sinninghe Damsté (2006), Archaeal tetraether membrane lipid fluxes in the northeastern Pacific and the Arabian Sea: Implications for TEX_{86} paleothermometry, *Paleoceanography*, *21*, PA4208, doi:10.1029/2006PA001279.

Yamamoto, M., Y. Shiraiwa, and I. Inouye (2000), Physiological responses of lipids in *Emiliania huxleyi* and *Gephyrocapsa oceanica* (Haptophyceae) to growth status and their implications for alkenone paleothermometry, *Org. Geochem.*, *31*, 799–811.

Yamamoto, M., A. Shimamoto, T. Fukuhara, Y. Tanaka, and J. Ishizaka (2012), Glycerol dialkyl glycerol tetraethers and TEX_{86} index in sinking particles in the western North Pacific, *Org. Geochem.*, *53*, 52–62.

Zabeti, N., P. Bonin, J. K. Volkman, I. D. Jameson, S. Guasco, and J. F. Rontani (2010), Potential alteration of $\mathbf{U}^{\boldsymbol{K'}}_{37}$ paleothermometer due to selective degradation of alkenones by marine bacteria isolated from the haptophyte Emiliania huxleyi, *FEMS Microbiol. Ecol.*, *73*(1), 83–94.

Zhang, Y. G., C. L. Zhang, X. L. Liu, L. Li, K. U. Hinrichs, and J. E. Noakes (2011), Methane Index: A tetraether archaeal lipid biomarker indicator for detecting the instability of marine gas hydrates, *Earth Planet. Sci. Lett.*, *307*, 525–534.

Zhang, Y. G., M. Pagani, and Z. Wang (2015), Ring Index: A new strategy to evaluate the integrity of TEX_{86} paleothermometry, *Paleoceanography*, *31*, 220–232, doi:10.1002/2015PA002848.

Zhu, C., S. G. Wakeham, F. J. Elling, A. Basse, G. Mollenhauer, G. J. Versteegh, M. Konneke, and K. U. Hinrichs (2016), Stratification of archaeal membrane lipids in the ocean and implications for adaptation and chemotaxonomy of planktonic archaea, *Environ. Microbiol.*, doi:10.1111/1462-2920.13289.